Topographic modulation on the layered circulation in South China Sea

Qibang Tang[12], Zhongya Cai[12], Zhiqiang Liu[3]

1 State Key Laboratory of Internet of Things for Smart City, Department of Ocean Science and Technology, University of Macau, China

2 Centre of Ocean Research in Hong Kong and Macau (CORE), Hong Kong, China

3. Department of Ocean Science and Engineering and Center for Complex Flows and Soft Matter Research, Southern University of Science and Technology, Shenzhen, China

Correspondence to: Zhongya Cai (zycai@um.edu.mo)

Abstract: The South China Sea (SCS) is the largest semi-enclosed marginal sea in western Pacific. It exhibits a unique vertically rotating cyclonic, anticyclonic, and cyclonic circulation in its upper, middle, and deep layers. Over slope topography, these layered currents interact and significantly shape the structure and intensity of the basin circulation. In this study, we employ process-oriented numerical simulations to investigate how upper-layer processes, characterized by greater magnitude and variability, influence the layered circulation over the irregular topographic slope. The simulations reveal that stronger upper intrusion from open ocean directly enhances upper layer circulation, which subsequently strengthens the middle and the deep slope currents. Vorticity dynamics illustrate that changes in the middle and deep slope current are largely related to the vertical stretching (ζ_DIV) induced by bottom geostrophic cross-isobath transport (CGT_b). As the upper-layer cyclonic slope current intensifies, it modulates the bottom pressure distribution, resulting in stronger negative ζ_DIV predominantly over the northwestern slope to intensify the middle anticyclone slope current. Similarly, for the deep cyclonic slope current, the CGT_b maintains downwelling in the northern part and upwelling over the southern slope. Over the southern slope, the strengthening of the positive CGT_b is induced by the increment of the advection of relative vorticity and planetary vorticity in water column, in which the middle layer has important contribution, but the upper layer has a minimal impact. Conversely, on the northern slope, the strengthening of the negative CGT_b is primarily influenced by the upper layer.

Keywords: Circulation dynamics; Layered circulation; Process-oriented simulation; Topographic modulation; Vertical coupling

39

1. **Introduction**

Marginal seas circulation plays crucial role in the mass transport and regional climate dynamics, with circulation patterns being strongly influenced by their unique topographic features (Millot 1999, Omstedt, Elken et al. 2004, Oey, Ezer et al. 2005, Gan, Li et al. 2006, Johns and Sofianos 2012). This topographic regulation results in intricate layered slope currents that flow in different directions at various depths (Yuan 2002, Wang, Xie et al. 2011, Lan, Zhang et al. 2013, Gan, Kung et al. 2022). These layered currents interact over slope topography, significantly shaping the structure and intensity of the overall circulation (Gan, Liu et al. 2016, Quan and Xue 2018). For instance, in the Gulf of Mexico, loop current eddies influence not just the upper-layer circulation but also the deep flow, illustrating the importance of vertical coupling in transferring energy and variability to deeper currents (Tenreiro, Candela et al. 2018). Understanding these dynamics helps elucidate the behavior of marginal sea's circulation (Liang, Spall et al. 2017, Zhu and Liang 2020, Olvera-Prado, Moreles et al. 2023).

The South China Sea (SCS) is the largest semi-enclosed marginal sea located in the tropical region. It exhibits a unique mean cyclonic, anticyclonic, and cyclonic (CAC) circulation in its upper, middle, and deep layers (Wang, Xie et al. 2011, Shu, Xue et al. 2014, Lan, Wang et al. 2015, Gan, Liu et al. 2016, Zhu, Sun et al. 2017). The strong upper layer circulation is driven by the Asia monsoon and Kuroshio intrusion from Luzon Strait (LS), while the middle and deep circulations are maintained by the outflux and deep intrusion through LS, respectively. Based on current understanding, the upper-layer influx through the Luzon Strait (LS) is induced by the Kuroshio Current as it passes through the strait (Nan et al., 2015). The middle-layer outflux and deep-layer intrusion, on the other hand, are largely driven by density differences caused by contrasting turbulent mixing intensities (e.g., Tian et al., 2009; Zhu et al., 2019; Zhou et al., 2023). Over the slope topography, the CAC circulation affects each other through the vertical coupling among them (Shu, Wang et al. 2018). For example, the study of Quan and Xue (2018) demonstrated that perturbations in the upper layer can transit through the water column and affect deeper circulation by altering layer thickness. This coupling is particularly evident over the strong boundary current that in the northern basin and along the western boundary. Numerical experiments by Wang et al. (2018) suggest that, although the basin-scale circulation is primarily driven by the LS overflow, upwelling patterns are essential in shaping the detailed structure of the deep-water circulation. Similar processes have been observed in other marginal seas as well (e.g., Testor et al., 2018; Wang et al., 2024; Xu et al., 2009; Olvera-Prado, Moreles et al. 2023).

Previous studies have advanced our understanding of the major features of the mean layered circulation and have highlighted the potential for strong coupling among layers,

particularly over sloping topography. However, the response of this circulation to changes in external forcings—particularly the strong upper ocean processes—and the specific mechanisms involved remain insufficiently understood. A comprehensive understanding of how topographically modulated vertical coupling over basin slopes influences the structure and intensity of mean circulation is crucial for exploring the long-term evolution of marginal sea circulation. For instance, Kuroshio intrusion has been observed to weaken with decadal variations, while upper ocean currents have shown acceleration in response to a warming climate (Peng et al., 2022; Chen et al., 2019; Nan et al., 2013). How the layered circulation in marginal seas responds to these changes remains unclear. This study employs process-oriented simulations to elucidate how upper-layer processes, which exhibit greater intensity and variability, influence layered circulation over the curved bottom slope in the SCS. The paper is organized as follows: Section 2 explains the configuration of the simulation. Section 3 offers the response of layered slope current intensity to the changes of the upper circulation. Section 4 explores the underlying physical mechanisms. Finally, Section 5 provides a summary of our findings.
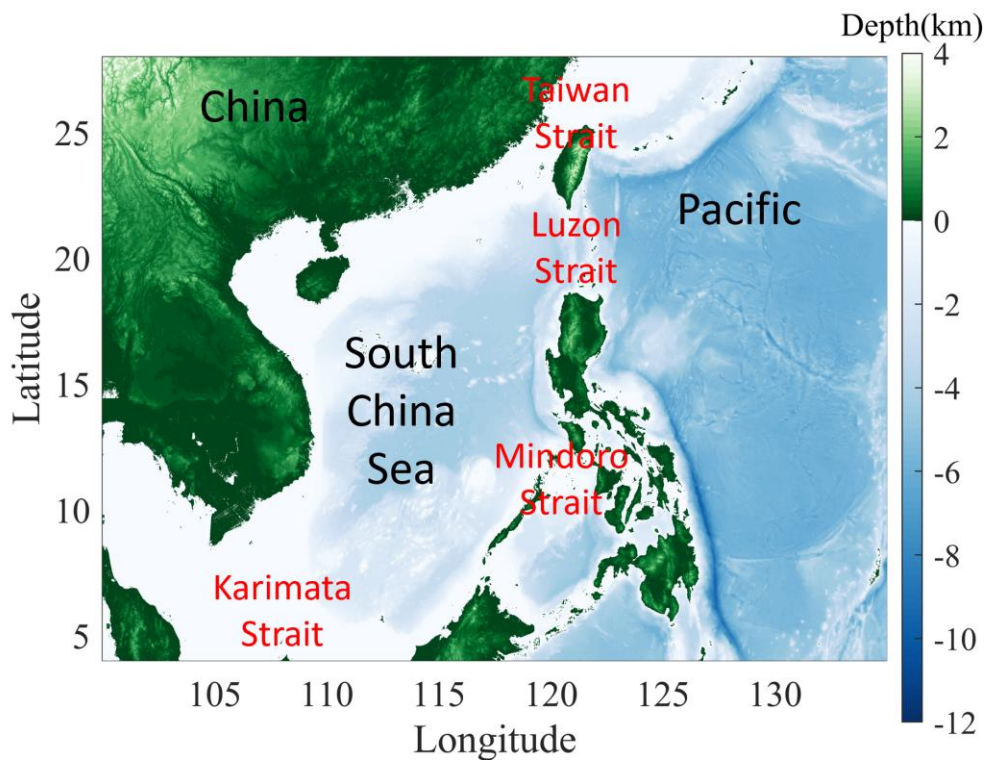
Figure1. Location and bathymetry (km) of the South China Sea, showing Luzon Strait, Taiwan Strait, Mindoro Strait, and Karimata Strait.

2. Methodology

Based on the Regional Ocean Modeling System (ROMS) (Shchepetkin and McWilliams

2005), we performed a three-dimensional process-oriented simulation in this study (Cai et al., 2023), which employs a simplified setup and allows for a clearer examination of the dynamical coupling between layers. Similar strategies have been applied in previous studies of SCS circulation (Chen and Xue 2014, Quan and Xue 2018, Wang, Du et al. 2018, Huang and Zhou 2022), and have provided valuable insights into specific dynamic mechanisms.

The model setup included a circular basin on the west representing the SCS and a rectangular basin on the east representing the Western Pacific Ocean. The slope in the SCS increases from 400 to 4000 m and the central basin has the depth of 4000 m. The SCS and Pacific basins were connected by a narrow strait (representing the LS) with a depth of 2500 m. The model employed a uniform horizontal grid with a 5 km resolution, and the vertical structure utilized stretched, terrain-following coordinates with 30 layers (Song and Haidvogel 1994) were adopted with 30 layers. Near the surface and bottom boundaries, the vertical resolution is refined with spacing of approximately 0.01, to reduce the spurious flow associated with numerical pressure gradient errors. In this simulation, the magnitude of the spurious flow is in the order of 10^{-2} m/s, which has limited impact on the results presented in this study. In the upper layer, an influx of 25 Sv and an outflux of 20 Sv were specified at the southeastern and northeastern boundaries of the open ocean, respectively (Figure 2c). The SCS was opened to the south with the depth of 400 m (Figure 2a), to allow the upper-layer intrusion to develop intrinsically during the simulation. To simulate the density differences and exchange currents in the middle and deep layers of the LS, the model incorporated variable contrasting mixing coefficients (K_v) between the SCS and the Western Pacific Ocean (Tian, Yang et al. 2009, Yang, Zhao et al. 2016). In the SCS and the western half of the LS, K_v values were set as $5 \cdot 10^{-4} m^2 s^{-1}$ between 500 and 1,500 m, $2 \cdot 10^{-3} m^2 s^{-1}$ below 1,500 m, and $5 \cdot 10^{-3} m^2 s^{-1}$ in the layer 500 m from the bottom. In the upper 500 m of SCS and LS, and throughout the entire water column of the open ocean, a background K_v of $2 \cdot 10^{-5} m^2 s^{-1}$ was applied. The K_v was designed based on observational work by Yang et al. (2016) and estimations by Wang et al. (2017) to form the circulation in the semi-enclosed middle and deep layers. Then, simulations were conducted to explore the response of the layered slope current, particularly in the semi-enclosed middle and deep layers, to changes in the upper-layer circulation. While it may be viewed as parameter tuning, our intention was not to simulate the mixing generation mechanisms explicitly, but rather to approximate the existing background structure that sustains the observed layered circulation. A zonal wind stress with meridional variations was applied over the open ocean, while the atmospheric buoyancy flux over the SCS was simplified by setting it to zero. This model simplifies the configurations to focus on the fundamental dynamics of the system. While these simplifications are essential for isolating key mechanisms, they may not capture the complexity of real-world conditions, potentially limiting its

134 quantitative applicability to realistic processes.

135   The model was initialized with horizontally uniform temperature and salinity profiles

136 derived from the mean data of the World Ocean Atlas, averaged over the region west of the LS.

137 The simulation ran for 25 years, with the analysis was conducted on the results from the final

138 5 years average after the layered circulation reached a stable state.

139

140
141
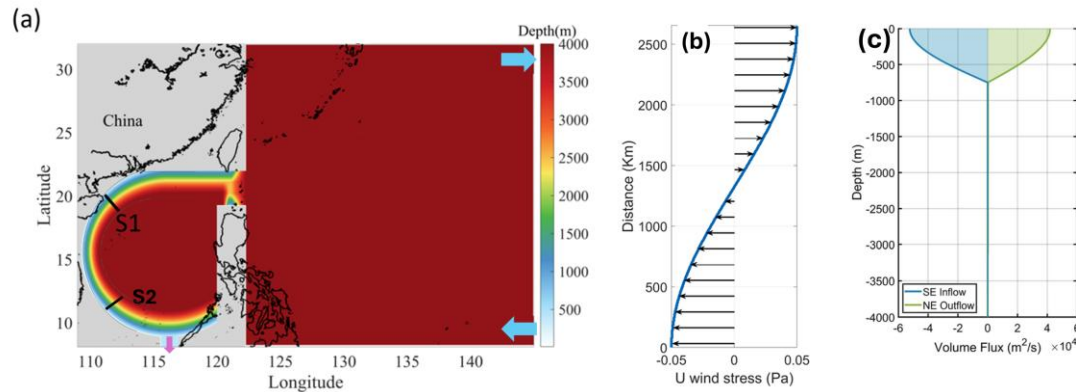
142 Figure 2. (a) The topography and geometry used in the idealized process-oriented simulation.
143 The black lines show the realistic surrounding coastline. S1 and S2 are two vertical sections for
144 showing slope current. (b) Distribution of the wind stress. (c) Vertical profile of the volume
145 inflow/outflux (m^2/s) through the southern/northern part of the eastern boundary
146

3. Results

148   In the LS, the influx occurs in the upper and deep layers, while the outflux occurs in the

149 middle layer between them (Figure 3b). The upper intrusion is intrinsically linked to the western

150 boundary current in the open ocean, i.e. Kuroshio Current. In the middle and bottom layers, the

151 exchange currents are primarily related to the density differences between the South China Sea

152 (SCS) and the Pacific. Although the initial temperature and salinity distributions are horizontally

153 uniform, the intensified turbulent mixing within the deep SCS basin gradually leads to a density

154 difference between the two sides of the LS. Specifically, the deep SCS exhibits lower density

155 compared to the Pacific basin (Figure S1). Under the density difference, the westward pressure

156 gradient was formed that drives the deep intrusion from the open ocean towards the SCS. Those

157 features are consistent with established understandings from previous studies (Wang, Xie et al.

158 2011). Associated with the simulated layered exchanging current, the layered circulations

159 developed inside the SCS basin. The upper, middle, and deep layers exhibit circulation in

160 cyclonic, anticyclonic, and cyclonic directions, respectively (Figure S1). The horizontally

161 averaged vorticity features with the positive-negative-positive values in the respective depth of

162 the basin (Figure 3b).
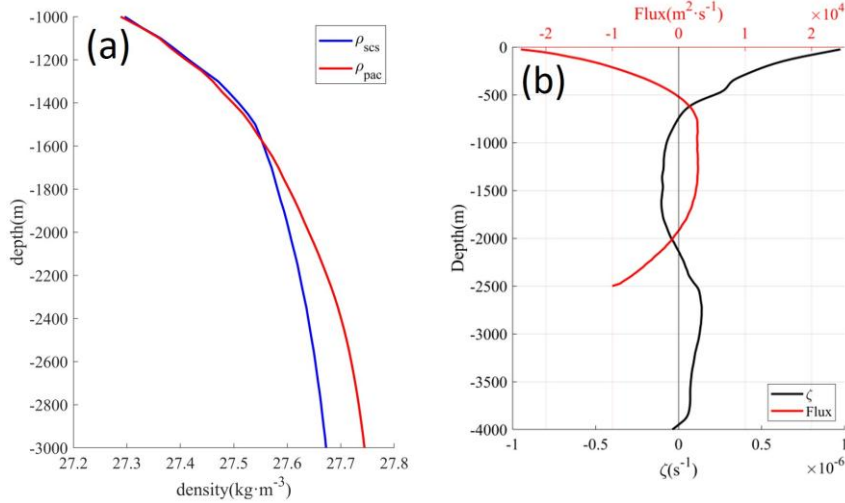
Figure 3. (a) Vertical profile of domain averaged density ρ (kg·m^{-3}) in SCS and Pacific between 1000m to 3000m. (b) Black line shows the vertical profile of the SCS basin-averaged vorticity (s^{-1}) and the red line shows the flux through LS (m^2·s^{-1}). The positive/negative vorticity represents the cyclonic/anticyclonic circulation, and the positive/negative value flux represents the outflux/influx through LS.

To investigate how the changes in upper layer current modulate the layered circulation, additional numerical experiments were conducted by adjusting the northeastern outflux to 22Sv, 23Sv and 24Sv, thus the upper LS intrusion was adjusted to 3Sv (Case_U3), 2Sv (Case_U2) and 1Sv (Case_U1). In these scenarios, the middle and deep exchanging currents, which were primarily sustained by the contrasting densities between the SCS and the open ocean, remained relatively unchanged (Figure 4a). Inside the basin, the enhancement of the upper layer inflow directly intensified the upper layer cyclonic circulation (Figure 4 c-f). And subsequently strengthened the middle anticyclonic slope current, particularly in the northwestern part of the basin (transect S1, Figure 4c, d). Additionally, although not directly connected to the upper layer, the deep cyclonic slope current also exhibited increased strength (Figure 4c-f). Using the domain-averaged vorticity as an indicator, it was observed that the intensification of the upper layer circulation resulted in a 10% increase in the intensity of the middle anticyclonic circulation and a 27% increase in the deep cyclonic circulation (Figure 4b). Given that only the upper layer circulation is directly amplified by the upper intrusion, the remote influence from upper layer processes over the basin slope significantly impacts the intensity of the layered circulation, which was explored below.

187

188

189
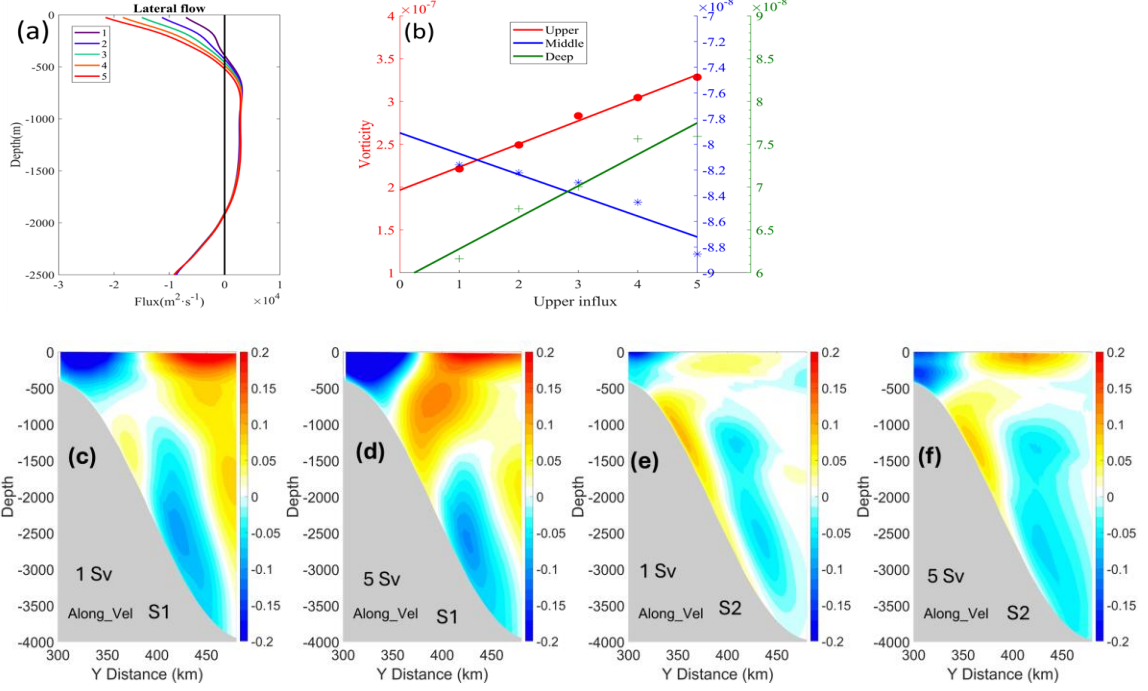
190 **Figure 4**. (a) Vertical profile flux across the LS under varying upper layer influx. (b) Changes
191 in the basin-averaged vorticity between 0-500 m (Upper), 1000-2000 m (Middle) and 3000-
192 4000 m (Deep) with different upper influx. (c-f) The along-slope current ($m \cdot s^{-1}$) over the
193 section S1 and S1 in Standard case (upper intrusion is 5 Sv) and Case_U1 (upper LS intrusion
194 is 1Sv), respectively. The locations of the two transects are shown in Figure 1a. The transect
195 locations are indicated in Figure 1a. Positive values represent anticyclonic flow, while negative
196 values indicate cyclonic flow.

197

198

199 **4. Discussion**

200

201 To understand how the upper layer processes modulate the layered current over the slope,

202 we first investigated the layered-integrated vorticity budget for each layer (Gan, Liu et al. 2016,

203 Cai, Chen et al. 2023):

204 $$\overbrace{\int_A [\nabla \times \int_{H_1}^{H_2} (\overrightarrow{PGF})\,dz]dA}^{\zeta\_PGF} + \overbrace{\int_A [\nabla \times \int_{H_1}^{H_2} (\overrightarrow{ADV})\,dz]dA}^{\zeta\_ADV} + \overbrace{\underbrace{\int_A \left[-f\nabla \cdot \int_{H_1}^{H_2} (\overrightarrow{V}_h)\,dz\right]dA}_{\zeta\_DIV} + \underbrace{\int_A \left[-\beta \cdot \int_{H_1}^{H_2} (v)\,dz\right]dA}_{\zeta\_BETA}}^{\zeta\_COR} +$$

205 $$\overbrace{\int_A [\nabla \times \int_{H_1}^{H_2} (\overrightarrow{HVIS})\,dz]dA}^{\zeta\_HVIS} + \overbrace{\int_A [\nabla \times \int_{H_1}^{H_2} (\overrightarrow{VVIS})\,dz]dA}^{\zeta\_VVIS} = 0 \quad (1)$$

206 where $\overrightarrow{PGF}$ is pressure gradient force, $\overrightarrow{ADV}$ is nonlinear advection, $\overrightarrow{HVIS}$ and $\overrightarrow{VVIS}$ are the

207 horizontal and vertical turbulent viscosity, respectively. COR is the Coriolis force and the

208 domain-integrated ζ_COR represents the lateral planetary vorticity flux. The H_1 and H_2

209 represent the bottom and upper depth of each layer, respectively. Inside the basin, the ζ_COR

210 can be further decomposed into the vertical stretching induced by the divergence of the

211 horizontal flow (ζ_DIV) and β effect of the meridional current (ζ_BETA).

The circulation in SCS is primarily governed by geostrophic balance, manifested as ζ_COR balanced by the ζ_PGF in both layers. It suggests that the mean cyclonic/anticyclonic circulation is related to the lateral planetary vorticity influx/outflux (Figure 5) (Cai and Gan 2019, Cai, Chen et al. 2023). Consequently, the strengthening of the upper LS intrusion directly intensifies the upper layer cyclonic slope current by providing more positive planetary vorticity flux. In the semi-enclosed middle and deep layers, the vorticity input is mainly provided by the ζ_DIV, as also highlighted in the previous studies (Zhu, Sun et al. 2017, Wang, Du et al. 2018, Cai, Chen et al. 2023). The positive ζ_DIV in the upper and deep layers reflects the downward and upward flux, which squeeze the middle layer and provide the negative vertical flux (negative ζ_DIV) for the anticyclonic circulation. Therefore, the intensification of the middle and deep slope currents is largely attributed to vertical stretching over the basin slope.
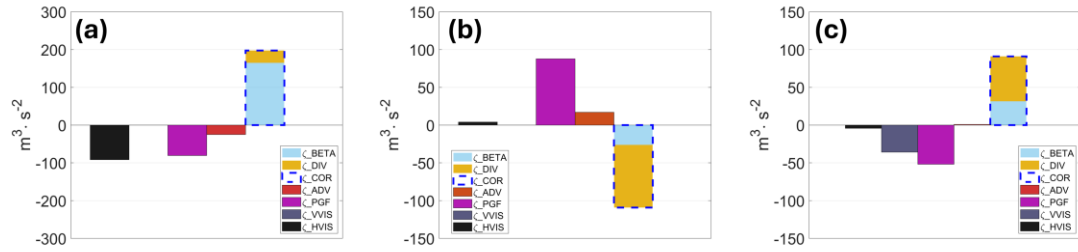
Figure 5. The layered-integrated vorticity budget (Equation 1) for the standard case in the layers of (a) 0–500, (b) 1,000–2,000, and (c) 2,500–4,000 m.

a. Intensification of middle anticyclonic slope current

For the middle anticyclonic slope current, the negative middle-layered ζ_DIV (ζ_DIV_M) mainly occurs over the northwestern slope (Figure 6a), where a relatively strong anticyclonic slope current is observed. In this area, the upper layer generally exhibits positive ζ_DIV (ζ_DIV_U), indicating downward squeezing from the upper layer that helps maintain the middle anticyclonic slope current (Figure 6 b). The increased squeezing from the upper slope current is expected to intensify the middle anticyclonic slope current (Figure 4 c, d). Since the stretching/squeezing imposed on the slope current is closely related to the vertical motion (Liang, Spall et al. 2017), the mean vertical motions over the slope can be understood as follows:

$$\overline{w} = -\nabla_h \cdot \int_{-H}^{z} \vec{\overline{V}}_h dz \approx -\nabla_h \cdot \int_{-H}^{z} \vec{\overline{V}}_{h\_geo} dz - \nabla_h \cdot \int_{-H}^{z} \vec{\overline{V}}_{h\_vis} dz$$

$$= \overbrace{-(\bar{v}_{b\_geo} H_y + \bar{u}_{b\_geo} H_x)}^{CGT_b} + \underbrace{\frac{\beta}{f} \int_{-H}^{z} \bar{v}_{geo} dz}_{\beta\ effect} \overbrace{- \nabla_h \cdot \int_{-H}^{z} \vec{\overline{V}}_{h\_vis} dz}^{Fric} \quad (2)$$

where H is the topography, $\_geo$ represents the geostrophic component of the horizontal

242 current, which is maintained by the distribution of bottom pressure. _vis represent the vertical

243 viscosity component. H_x and H_y are the horizontal gradients of the bottom slope, $\overline{u}_{b\_geo}$ and

244 $\overline{v}_{b\_geo}$ are the bottom geostrophic currents. When the current flows over the slope, the bottom

245 pressure distribution interacts with the curved topography and the resulting geostrophic cross-

246 isobath transport (CGT_b) to influence the vertical motions over the slope. The $Fric$ represent

247 the effect of the bottom Ekman pumping that induced by the bottom stress of the slope current.

248 Generally, the CGT_b largely governs the mean vertical motion over northwestern slope, which

249 in turn squeezes and stretches the middle and upper slope currents. This process is crucial in

250 maintaining the vorticity input through ζ_DIV (Figure 6 d), thereby sustaining the dynamics of

251 the slope currents.

252   Associated with the intensification of the upper layer cyclonic slope current, the stronger

253 slope current modulates the bottom pressure distribution over the slope, leading to stronger

254 vertical squeezing (ζ_DIV) within the water column. The increase in squeezing gradually

255 deepens the isopycnal surface and strengthens the middle anticyclonic slope current (Figure 6e).

256

257
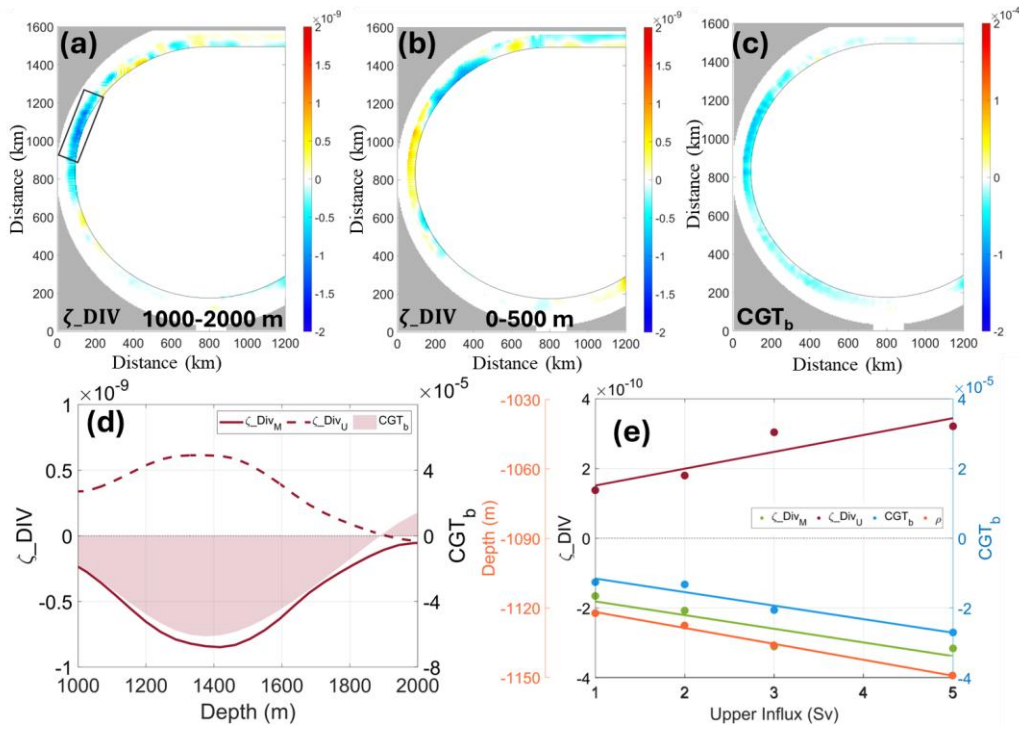
Figure 6. (a-c) ζ_DIV integrated between 1000-2000 m (ζ_DIV$_M$), 0-500 m (ζ_DIV$_U$), and
CGT_b over the region of middle anticyclonic slope current between 1000-2000 m. The black
line indicates the 2000 m isobath line. (d) Change of the ζ_DIV integrated between 100-2000 m
(ζ_DIV$_M$), between 0-500 m (ζ_DIV$_U$) with the depth over the northwestern slope. (e) Changes
of the ζ_DIV$_M$, ζ_DIV$_U$, CGT$_b$ and the depth of isopycnal surface of 1027.4 kg/m³ with different
upper LS influx. (d) and (e) was plotted using the data averaged over the region of black box
in (a)

265

266

b. Intensification of the deep cyclonic slope current

267

268   For the deep cyclonic slope current, the deep ζ_DIV (ζ_DIV$_D$) features a downward flux

269 (negative value) over the northern slope and upward flux (positive value) over the southern part

270 (Figure 7a, d). It suggests the sinking from the northern basin and upwelling from the southern

271 basin would sustain the abyssal cyclonic circulation. Same as the middle anticyclonic slope

272 current, the ζ_DIV$_D$ is. For the deep layer, the viscosity term has an important effect in the

273 vorticity budget (Figure 5c). Similarly, the $Fric_D$ term contributes to the deep ζ_DIV$_D$ and is

274 characterized by a relatively uniform downward motion (Figure 7d). However, the primary

275 pattern and magnitude of the ζ_DIV$_D$ are largely controlled by the CGT_b that the pressure

276 distribution maintained the mean downwelling in the northern side and the upwelling over the

277 southern slope (Figure 7b, d). Since the $Fric_D$ is induced by the bottom frictional stress as

278 response to the deep layer slope current, while the bottom pressure is modulated by the motions

279 of water in the entire water column above it, we further examine the maintenance of the bottom

280 pressure over the slope.

281   To explain the maintenance of the bottom pressure distribution, the vertical integrated

282 vorticity dynamic was employed (Gan, Liang et al. 2013, Cai and Gan 2021):

283
$$\overbrace{\nabla \times \int_{-H}^{0}(\overrightarrow{PGF})\,dz}^{\Omega\_PGF} + \overbrace{\nabla \times \int_{-H}^{0}\left(\overrightarrow{ADV}\right)dz}^{\Omega\_ADV} + \underbrace{\beta \int_{-H}^{0} v\,dz}_{\Omega\_BETA} - \overbrace{\nabla \times \int_{-H}^{0}(\overrightarrow{VIS})\,dz}^{\Omega\_VIS} = 0 \qquad (3)$$

284 Where $\Omega\_PGF = \nabla \times \int_{-H}^{0}(\overrightarrow{PGF})\,dz = -(\bar{v}_{b\_geo}H_y + \bar{u}_{b\_geo}H_x)$, thus represents the effect of CGT_b.

285 It illustrates that the bottom pressure distribution is maintained by the nonlinear advection of

286 relative vorticity (Ω_ADV), advection of planetary vorticity (Ω_BETA), and net viscosity of the

287 current flowing over the slope topography. Among them, the Ω_BETA and Ω_ADV play the

288 major role in sustaining the bottom pressure distribution of the deep cyclonic slope current

289 (Figure 8 c, d).

290
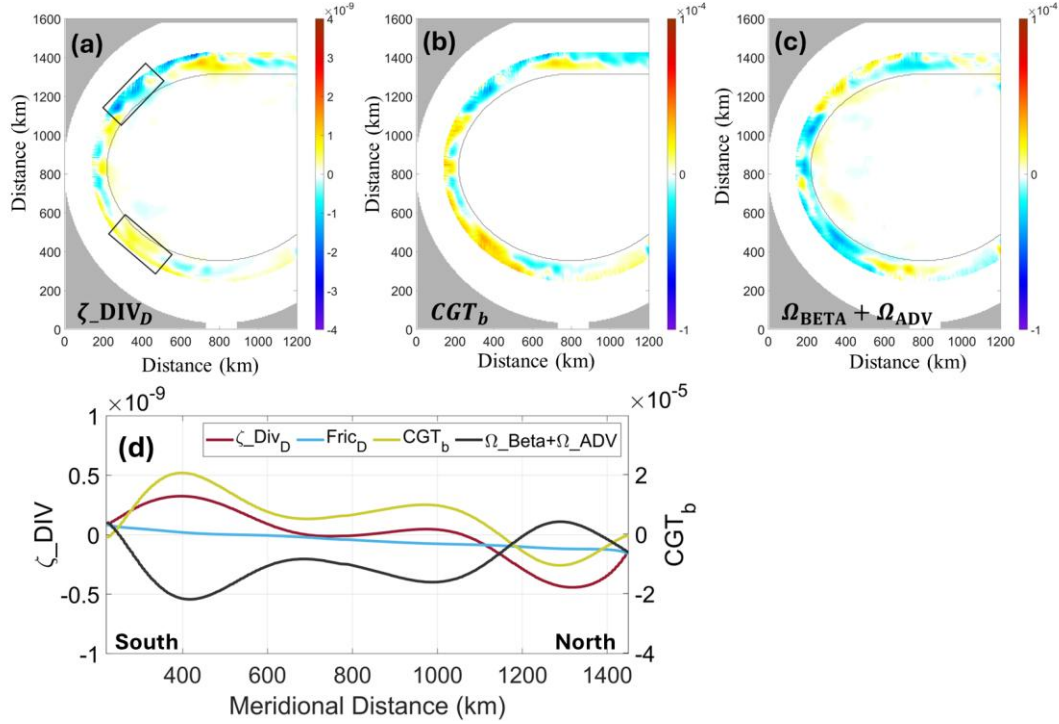
Figure 7 (a-c) ζ_DIV integrated below 3000 m of the deep cyclonic slope current (ζ_DIV_D), CGT_b and $\Omega\_BETA + \Omega\_ADV$ over the region of middle anticyclonic slope current below 3000 m. The black line indicates the 4000 m isobath line. (d) Meridional changes of the ζ_DIV_D, $Fric_D$, CGT_b and $\Omega\_BETA + \Omega\_ADV$ over the slope.

As the upper intrusion intensifies, the bottom pressure distribution adjusts in response to changes in the layered circulation, resulting in a gradual strengthening of the negative CGT_b over the northern slope and positive CGT_b over the southern part (Figure 8 a-b). Over the southern slope (Figure 8a), the strengthening of the positive CGT_b is induced by the increase of the $\Omega\_BETA + \Omega\_ADV$ in the water column, in which the middle layer [$\Omega\_BETA + \Omega\_ADV$ (M)] provides approximately 40% of the total strengthening trend, while the upper layer [$\Omega\_BETA + \Omega\_ADV$ (U)] has a negligible impact. Conversely, over the northern slope, the strengthening of the $\Omega\_BETA + \Omega\_ADV$ is primarily influenced by the upper layer, with the middle layer has the negative effect (Figure 8b). Thus, the intensification of downward CGT_b over the northern slope is directly modulated by the strengthening of the upper cyclonic slope current, while the intensification of upward CGT_b over the southern slope is mainly driven by the strengthening of the middle anticyclonic slope current. These changes in CGT_b enhance deep stretching, thereby strengthening the deep cyclonic slope current accordingly (Figure 8c).

311

312

313
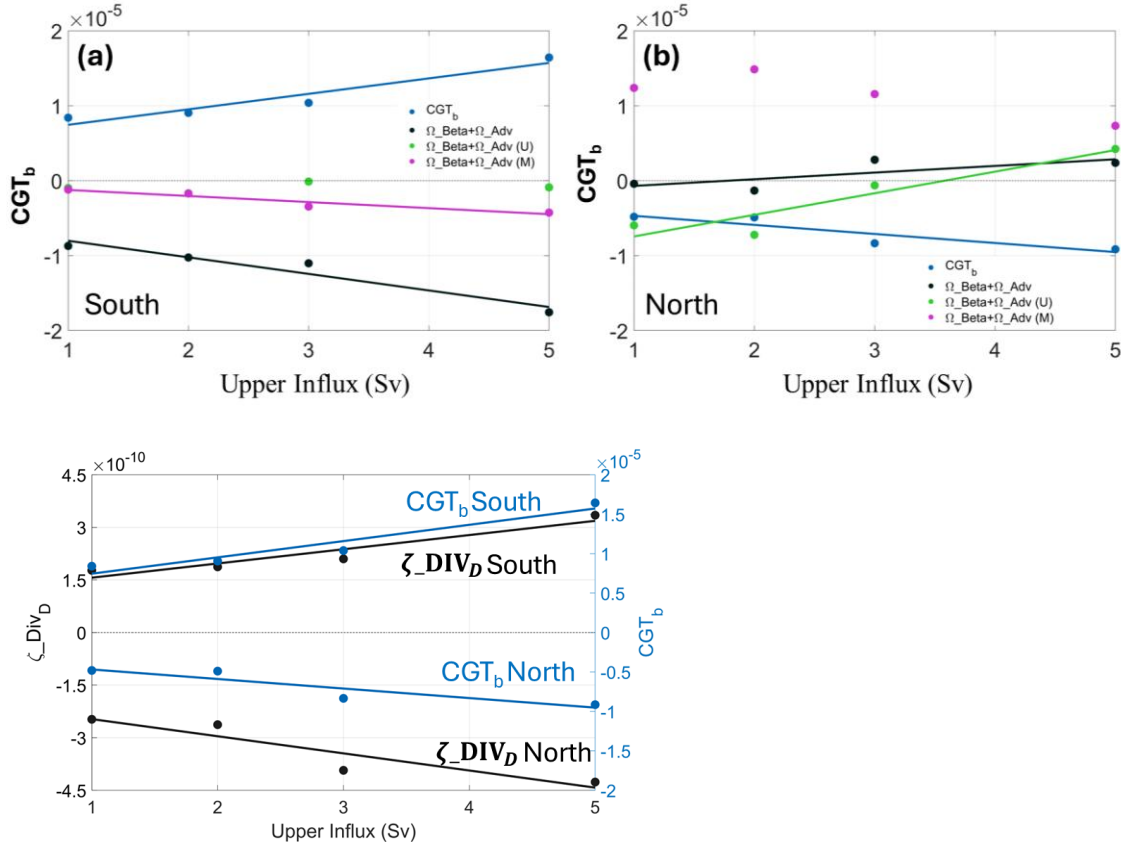
314 **Figure 8**. (a) Changes of the CGT_b, $\Omega_{Beta} + \Omega_{Adv}$ in the total water column, $\Omega_{Beta} + \Omega_{Adv}$ in the
315 layer between 0-500 m ($\Omega_{Beta\_U} + \Omega_{Adv\_U}$), $\Omega_{Beta} + \Omega_{Adv}$ in the between 1000-2000 m
316 ($\Omega_{Beta\_M} + \Omega_{Adv\_M}$) over the southern slope (black box in Figure 8a). (b) same as (a) but over
317 the northern slope (black box in Figure 8a). (c) Change of the CGT_b and ζ_DIV_D over the
318 northern and southern slope.

319

320

5. Summary

322   Marginal sea circulation plays a crucial role in mass transport and regional climate
323 dynamics. Through process-oriented numerical simulations, we examined how upper-layer
324 processes, which are characterized by greater intensity and variability, impact the layered
325 circulation over the curved bottom slope in SCS. The primary goal of our study is to provide
326 theoretical insights into the mechanisms driving layered circulation and their response to
327 changes in upper-layer motions. The results underscore the intricate balance between
328 topographical features and oceanic circulation. These insights have broad applicability to
329 understanding similar processes and phenomena in other regions, and help to predict the
330 behavior of marginal sea circulation under varying forcings conditions.

331   The numerical experiments show that the simulated layered exchange currents through the
332 LS introduce lateral planetary vorticity flux and facilitate the development of a layered basin

circulation within the SCS. Inside the basin, the intensification of upper-layer inflow directly enhances the upper-layer cyclonic circulation, which in turn strengthens the middle anticyclonic slope current, particularly in the northwestern part of the basin. Furthermore, even though the deep cyclonic slope current is not directly connected to the upper layer, it also exhibits increased strength. Using domain-averaged vorticity as an indicator, it was found that the intensification of the upper-layer circulation resulted in the increase in the intensity of the middle anticyclonic circulation and deep cyclonic circulation.

The vorticity dynamics illustrate that the changes in the middle and deep slope current is largely related to the vertical stretching over the slope (ζ_DIV). When the current flows over the slope, the bottom pressure distribution interacts with the curved topography and the resulting geostrophic cross-isobath transport (CGT_b) influences the vertical motions. For the middle anticyclonic slope current, the negative middle ζ_DIV predominantly occurs over the northwestern slope, where a relatively strong anticyclonic slope current is present. As the upper-layer cyclonic slope current intensifies, it modulates the bottom pressure distribution over the slope, providing stronger vertical squeezing ζ_DIV within the water column, which gradually strengthens the middle anticyclonic slope current. For the deep cyclonic slope current, the deep ζ_DIV is also largely controlled by the CGT_b over the slope, with the pressure distribution maintaining downwelling flows in the northern part and upwelling over the southern slope. Over the southern slope, the strengthening of the positive CGT_b is induced by the increase of the nonlinear advection of relative vorticity and planetary vorticity in the entire water column, in which the middle layer provides approximately 40% of the total strengthening trend, while the upper layer has a negligible impact. Conversely, on the northern slope, the strengthening of the negative CGT_b is primarily influenced by the upper layer, with the middle layer has the negative effect.

The results from this process-oriented study offered clear processes for understanding vertical coupling among circulation layers. The motions in one layer influence others by modifying the along-slope pressure distribution and corresponding stretching, thereby facilitating inter-layer interaction. It should be noted that those understandings are based on process-oriented simulation with simplified configurations. Based on the obtained understanding, a more realistic simulation in our following study, incorporating detailed topography and external forcings, will offer more quantitative insights and help further validate and extend the findings presented here. In addition to the processes revealed in this study, other mechanisms, such as the Neptune Effect involving the eddy-slope interaction (e.g., Holloway, 1987, Stewart et al., 2024), may also play a role in influencing circulation dynamics in marginal seas like the SCS. It will be incorporated into our future investigations to improve understanding.

369

370

Data availability. All data and source code used in this paper are available at https://doi.org/10.5281/zenodo.15081223.

373

374 Author contributions. QT conducted the investigation, developed the methodology, and carried

375 out the writing (original draft preparation). ZC was responsible for the conceptualization,

376 supervision, and writing (review and editing). ZL was responsible for the conceptualization and

377 writing (review and editing).

378

379 Competing interests. The contact author has declared that none of the authors has any

380 competing interests.

381

382 *Acknowledgement*

383   This work was supported by National Natural Science Foundation of China

384 (42376024, 42276004), the Science and Technology Development Fund, Macau SAR

385 (File/Project no. 001/2024/SKL, 0040/2023/R1A1), and The Center for Ocean

386 Research in Hong Kong and Macau (CORE, EF014/FST-CZY/2023/HKUST). The

387 work described in this paper was substantially supported by a grant from the Research

388 Grants Council of the Hong Kong Special Administrative Region, China (AoE/P-

389 601/23-N). CORE is a joint research centre for ocean research between Laoshan

390 Laboratory and HKUST. This work was performed in part at the SICC, which is

391 supported by the SKL-IOTSC, University of Macau.

392
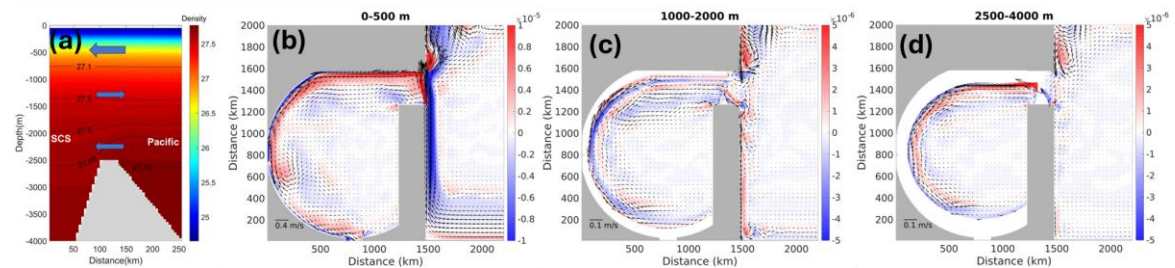
394 Figure S1. (a) Vertical transect of density (represented by color shading and contour lines)

395 across the Luzon Strait. The left side represents the SCS basin, while the right side corresponds

396 to the Pacific basin. Schematic arrows indicate the direction of the exchange flow between the

397 two basins. (b-c) The horizontal circulation (arrows) and depth averaged vorticity (color) of (b)

398 upper layer 0-500 m, (c) middle layer 1000-2000 m and (d) deep layer 2500-4000 m in the

399 standard case.

Reference

Cai, Z., D. Chen and J. Gan (2023). "Formation of the layered circulation in South China Sea with the mixing stimulated exchanging current through Luzon Strait." Journal of Geophysical Research: Oceans

Cai, Z. and J. Gan (2019). "Coupled External-Internal Dynamics of Layered Circulation in the South China Sea: A Modeling Study." Journal of Geophysical Research: Oceans 124(7): 5039-5053.

Cai, Z. and J. Gan (2021). "Dynamics of the Layered Circulation Inferred from Kinetic Energy Pathway in the South China Sea." Journal of Physical Oceanography 51(5): 1671-1685.

Chen, G. and H. Xue (2014). "Westward intensification in marginal seas." Ocean Dynamics 64(3): 337-345.

Gan, J., H. Kung, Z. Cai, Z. Liu, C. Hui and J. Li (2022). "Hotspots of the stokes rotating circulation in a large marginal sea." Nat Commun 13(1): 2223.

Gan, J., H. Li, E. N. Curchitser and D. B. Haidvogel (2006). "Modeling South China Sea circulation: Response to seasonal forcing regimes." Journal of Geophysical Research 111(C6).

Gan, J., L. Liang and H. San Ho (2013). "Dynamics of Intensified Downwelling Circulation over a Widened Shelf in the Northeastern South China Sea." Journal of Physical Oceanography 43(1): 80-94.

Gan, J., Z. Liu and C. R. Hui (2016). "A Three-Layer Alternating Spinning Circulation in the South China Sea." Journal of Physical Oceanography 46(8): 2309-2315.

Holloway (1987): Systematic forcing of large-scale geophysical flows by eddy-topography interaction, Journal of Fluid Mechanics.

Huang, -. R. X. and -. H. Zhou (2022). "- Circulation in the South China Sea is in a state of forced oscillation: Results from a simple reduced gravity model with a closed boundary." - Acta Oceanologica Sinica - 41(- 7): - 1.

Johns, W. E. and S. S. Sofianos (2012). "Atmospherically Forced Exchange through the Bab el Mandeb Strait." Journal of Physical Oceanography 42(7): 1143-1157.

Lan, J., Y. Wang, F. Cui and N. Zhang (2015). "Seasonal variation in the South China Sea deep circulation." Journal of Geophysical Research: Oceans 120(3): 1682-1690.

Lan, J., N. Zhang and Y. Wang (2013). "On the dynamics of the South China Sea deep circulation." Journal of Geophysical Research: Oceans 118(3): 1206-1210.

Liang, X., M. Spall and C. Wunsch (2017). "Global Ocean Vertical Velocity From a Dynamically Consistent Ocean State Estimate." Journal of Geophysical Research: Oceans 122(10): 8208-8224.

Millot, C. (1999). "Circulation in the western Mediterranean Sea." Journal of Marine Systems 20(1-4): 423-442.

430 Oey, L., T. Ezer and H. Lee (2005). "Loop Current, rings and related circulation in the Gulf of Mexico: A review of

431 numerical models and future challenges." Geophysical Monograph-American Geophysical Union 161: 31.

432 Olvera-Prado, E. R., E. Moreles, J. Zavala-Hidalgo and R. Romero-Centeno (2023). "Upper–Lower Layer Coupling

433 of Recurrent Circulation Patterns in the Gulf of Mexico." Journal of Physical Oceanography 53(2): 533-550.

434 Omstedt, A., J. Elken, A. Lehmann and J. Piechura (2004). "Knowledge of the Baltic Sea physics gained during the

435 BALTEX and related programmes." Progress in Oceanography 63(1-2): 1-28.

436 Quan, Q. and H. Xue (2018). "Layered model and insights into the vertical coupling of the South China Sea

437 circulation in the upper and middle layers." Ocean Modelling 129: 75-92.

438 Shchepetkin, A. F. and J. C. McWilliams (2005). "The regional oceanic modeling system (ROMS): a split-explicit,

439 free-surface, topography-following-coordinate oceanic model." Ocean Modelling 9(4): 347-404.

440 Shu, Y., Q. Wang and T. Zu (2018). "Progress on shelf and slope circulation in the northern South China Sea."

441 Science China Earth Sciences 61(5): 560-571.

442 Shu, Y., H. Xue, D. Wang, F. Chai, Q. Xie, J. Yao and J. Xiao (2014). "Meridional overturning circulation in the

443 South China Sea envisioned from the high-resolution global reanalysis data GLBa0.08." Journal of Geophysical

444 Research: Oceans 119(5): 3012-3028.

445 Song, Y. and D. Haidvogel (1994). "A semi-implicit ocean circulation model using a generalized topography-

446 following coordinate system." Journal of Computational Physics 115(1): 228-244.

447 Stewart et al. (2024): Formation of eastern boundary undercurrents via mesoscale eddy rectification, Journal of

448 Physical Oceanography.

449 Tenreiro, M., J. Candela, E. P. Sanz, J. Sheinbaum and J. Ochoa (2018). "Near-Surface and Deep Circulation

450 Coupling in the Western Gulf of Mexico." Journal of Physical Oceanography 48(1): 145-161.

451 Tian, J., Q. Yang and W. Zhao (2009). "Enhanced diapycnal mixing in the South China Sea." Journal of Physical

452 Oceanography 39(12): 3191-3203.

453 Wang, A., Y. Du, S. Peng, K. Liu and R. X. Huang (2018). "Deep water characteristics and circulation in the South

454 China Sea." Deep Sea Research Part I: Oceanographic Research Papers 134: 55-63.

455 Wang, G., S.-P. Xie, T. Qu and R. X. Huang (2011). "Deep South China Sea circulation." Geophysical Research

456 Letters 38(5): n/a-n/a.

457 Yang, Q., W. Zhao, X. Liang and J. Tian (2016). "Three-Dimensional Distribution of Turbulent Mixing in the South

458 China Sea." Journal of Physical Oceanography 46(3): 769-788.

459 Yuan, D. (2002). "A numerical study of the South China Sea deep circulation and its relation to the Luzon Strait

460 transport." Acta Oceanologica Sinica(2): 187-202.

461 Zhu, Y. and X. Liang (2020). "Coupling of the Surface and Near-Bottom Currents in the Gulf of Mexico." J Geophys

462 Res Oceans 125(11): e2020JC016488.

463 Zhu, Y., J. Sun, Y. Wang, Z. Wei, D. Yang and T. Qu (2017). "Effect of potential vorticity flux on the circulation in

464 the South China Sea." Journal of Geophysical Research: Oceans 122(8): 6454-6469.

465

466